Dual arm electrical transmission line robot: motion through straight and jumper cable

C. M. Shruthi, A. P. Sudheer & M. L. Joy

Published online: 02 May 2019.

Submit your article to this journal ↗

Article views: 1285

View related articles ↗

View Crossmark data ↗

Citing articles: 3 View citing articles ↗

Taylor & Francis
Taylor & Francis Group

REGULAR PAPER

OPEN ACCESS

Check for updates

Dual arm electrical transmission line robot: motion through straight and jumper cable

C. M. Shruthi ⓘ, A. P. Sudheer ⓘ and M. L. Joy ⓘ

Department of Mechanical Engineering, National Institute of Technology Calicut, Kozhikode, India

ABSTRACT

Ground-based high voltage electrical line inspection is one of the difficult and highly dangerous job as far as a manual worker is concerned. The transmission line inspection by robots avoids temporary interruption of power supply that affects the end user and transmission grid. Also, robot-based inspection reduces maintenance cost and hazards. The electrical line inspection is normally carried out using binoculars and rarely by helicopters in most of the countries because of the low cost. Wire traversing or aerial robots are being used in Japan, Canada, USA and Russia for inspecting and monitoring faults in transmission lines and towers. However, most of these robots require a lot of human effort for installation due to its weight and complex design. Cost of these robots is also very high. This paper presents the mechanical design, fabrication and testing of a novel, low cost, light weight and compact power transmission line inspection robot. This work also includes kinematic, static and dynamic analysis of various subsystems of robot. Proposed robot is capable of traversing on straight transmission line and jumper cables present in tension towers. The robot has 10 DoF dual arm for crossing operation and a base system to achieve the locomotion.

1. Introduction

Manual and helicopter based high voltage line inspection are common in most of the developing countries. Manual inspection in power transmission lines involves higher risk, and it is unsafe, hazardous, time consuming and an expensive approach [1–3]. Hence, the present trend is to replace humans with autonomous line inspection robot thereby reducing the number of accidents and improving the inspection efficiency. Remotely operated robots can also be used for the real-time inspection of power lines [4]. The major obstacles to be avoided are suspension towers, tension towers, spacers, dampers and insulators as shown in Figures 1 and 2. Crossing of tension towers is tougher compared to that of suspension towers due to the insulators along the line. Hence, the challenging issue is that the robot has to reposition itself from straight transmission line to jumper cable and then back to straight line. High voltage line inspection robots can also be used for inspecting structural and suspension cables on bridges, robotic surveillance along the cables, crop monitoring and forestry research [6].

1.1. Existing power-line inspection robots

The comprehensive study of most of the electrical transmission line inspection robots has been carried out and research gaps have been identified. However, only main robots are included in this manuscript. Power Transmission Line (PTL) robots are reviewed and summarized based on the main features such as live line, bundled conductors, obstacle avoidance, strain pylon bypassing, suspension pylon bypassing and pylon/line docking navigation. Eight PTL robots developed by various institutions with countries are listed in [7]. In review paper [8], latest trends and types of mobile robots for PTL are presented. A very few numbers of existing robots employed by the EPRI (Electric Power Research Institute) crosses suspension towers as well as tension towers [9]. Line-Scout is the most efficient line inspection robot developed by Hydro-Quebec Canada. Line scout can surmount obstacles by gripping the line with its arm frame which is designed for obstacle navigation and moving the wheel frame forward along with the centre frame [10–12]. It comprises of three subsystems: a wheel frame, a centre frame, and the arm frame. These sub-systems helpthe robot to cross the obstacle but not the tension towers. The limitations of this robot are that the robot is very heavy and does not cross the tension towers. Expliner [13], the robot developed by the Tokyo Institute of Technology, the Kansai Power Corporation and the HiBot Corporation Japan. It consists of wheels, wheel-frame and counterweight where counterweight is used to balance the motion. Smaller obstacles are crossed by the robot by rolling over them and larger obstacles by adjusting/balancing weight of the counterweight by lifting one set of wheels. When both the set of wheels are crossed beyond the obstacle,
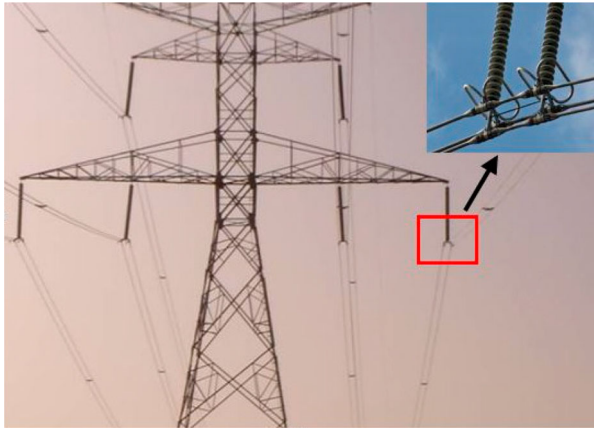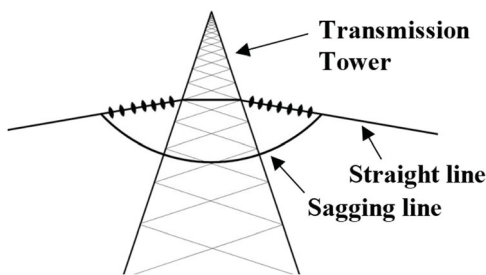
Figure 1. Suspension tower [5].

Figure 2. Line sketch of a Tension tower.

the robot continues to move along the straight power-line. The demerit of this robot is that the robot can run only on dual power-line. Cable crawler [14] is designed by ETH Zurich which traverses on a single cable by achieving complete freedom with less number of actuators. The cable crawler is teleoperated and is capable of continuous motion through the guide wires of the transmission tower. This robot is capable of traversing on slightly inclined cables and mast tops without adding any extra actuators in the robot structure. The major drawback of this design is the accessibility since it is limited just to the guide wire. Bipedal Line Walking Robot [15] is a robot developed by a team from Kunshan Institute of Industry Research and University of Hamburg. Bipedal Line Walking Robot is a 2PR robot which consists of three segments: a pair of legs, a waist and a body. There are two types of locomotion gaits associated with robot to traverse and cross small obstacles. One of the gait is a flipper stride in which lifting of legs is done in a striding motion and the other one is crawling stride in which shuffling of legs is done along the line. A hybrid robot [16] is a drone developed in China which is used for autonomic power line inspection. This robot is able to land on the overhead transmission line and to move along the same. When the robot comes across an obstacle, it vertically take off from the wire and fly over the obstacles to cross them. By using a 2D LRF and servo motor with an on-board embedded processor, the accurate pose of transmission line is robustly detected. Combined

with the trumpet-shaped undercarriage, the robot can robustly land on OGW and keep balance without the power of airscrews. There are some limitations for a drone: Drones have limited flight time and limited payload capacity. Weather conditions for flying a drone must be very calm and pleasant. Hence, drones cannot be operated during bad weather conditions like rain and snow-fall etc. An inspection robot [17] which is capable of inspecting and cleaning the power cable is developed by University of Georgia, USA. V-grooved wheels are used to grid the lines and avoid the smaller obstacles in this prototype. This robot has various features such as vision-based power line inspection, scrub-brush based cleaning, wireless control for remote operation, auto-stop safety and ability to manoeuvre around obstacles. Three robots [18] such as Portable Inspection Robot (PIR), Traversing Inspection Robot (TIR) and Climbing Inspection Robot (CIR) are developed by Wuhan University, China for straight line motion, crossing obstacles and crossing the tower junctions. The first robot PIR is able to move through the straight transmission line with obstacles, however it cannot cross the tower junctions. The second robot TIR is able to cross all kind of obstacles and it can also cross tower junctions with separate attachment in the tower structure. The third robot is CIR imitates the behaviour of animals for straight line motion and crossing the obstacles including the crossing of tower junctions. Another inspection robot [19] is developed by Mongolian University of Science and Technology, Mongolia. This robot can crawl and move through the transmission line and detect obstacles using camera and inspect using other kind of sensors. A mobile robot [20–36] is an obstacle avoidance robot developed by Robotics laboratory of Chinese Academy of Sciences (CAS) and Wuhan University for crossing tower junction and obstacles. This mobile robot consists of a body with two arms namely forearm and rear-arm for traversing and obstacles avoidance. A novel and fast visual obstacle recognition algorithm is proposed to detect the obstacles from the complex background accurately with less computational time. An autonomous inspection robot is introduced by [37–41] at University of Shanghai for Science and Technology, China. The robot developed is an inspection robot similar to CAS's which autonomously avoids obstacles on an 110 kV Power Transmission Line (PTL) with an obstacle avoidance planning method. In particular, this robot focused on supporting navigation along an inclined line with unstable counterbalancing. The inspection robot is composed of two arms and two-wheel claws which are used to imitate the monkey's motion. This robot has 13 DoF to imitate the monkey's motion and avoiding obstacles. This mobile robot is tested on an OGW of 500 kV tower for inspection. Position and force sensors are attached to the robot to identify the obstacles and to grasp the OGW. This robot will move through bridges which are integral part of torsion

tower junctions for crossing. A mobile robot platform [42] developed by Eletrobras-Cepel, Brazil for visually inspecting the external conditions of conductors and detecting internal faults in the Aluminium conductor steel-reinforced (ACSR) cables. Experiments are conducted on the electromagnetic interference and radio frequency interference (EMI and RFI) of the developed inspection robot in both laboratory and actual PTL environment. The robot cannot cross the obstacles. An inspection robot [43,44] developed by the University of KwaZulu-Natal, South Africa. The robot is made of a simple manipulator design that has 5 degrees of freedom. The robot can cross obstacles and towers by adjusting the angle between two arms having a V-shape.

An appropriate robot mechanism for both tension and suspension towers are not reported till now for transmission line inspection. Most of the existing line inspection robots are heavy, bulky with several complicated mechanisms and are costly. Most of the existing robots fails to cross tension towers due to the absence of appropriate mechanisms to cross jumper cables. It is also observed that the robots were not autonomous and needed manual operator to supervise the inspection operation. Moving through straight line and crossing through jumper cable are the main challenges in the development of the mechanism for high voltage line inspection.

The primary objective of the work is to develop an electrical transmission line robot which can traverse through straight-line wire and cross obstacles which can be used in both suspension and tension towers. This robot is equipped with the robotic arm and pulley mechanism for crossing and obstacle avoidance in the transmission lines. This paper also presents the synthesis of mechanism, kinematic and static analysis, dynamic analysis of the arm and robot, integration of subsystems and testing of robot in a fabricated transmission line setup.

2. Design of transmission line inspection robot mechanism

Robot mechanism is designed for Indian high voltage transmission lines. CAD model of the robot is shown in Figure 3. Robot consists of 3 subsystem namely mobile base, pulley mechanism and 10 DoF dual arm. Mobile base helps the robot to traverse on the transmission line, pulley mechanism and 10 DoF dual arm are the sub-systems which helps in crossing the obstacles and towers. The mobile base has the following subsystems: (1) two driving wheels and two idle wheels, (2) sliding mechanism with swing unit and engage-disengage unit and (3) locking mechanism with lock tab and the supporting wheel. Subsystems are given in detail in the following sections.
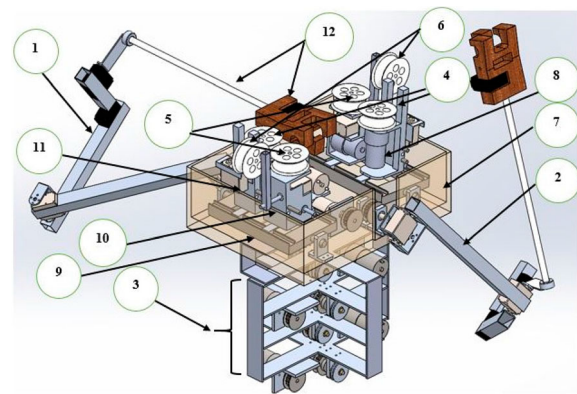
1.Arm1, 2.Arm2, 3.Pulley system, 4.Driving wheels, 5.Idle wheels, 6.Supporting wheels, 7.Robot base chassis, 8.Driving motor, 9.Pitch plate/Swing unit, 10. Motor mount A, 11.Motor mount B, 12.Nylon rod and gripper hook.

Figure 3. CAD model of the dual arm robot.

2.1. Working of the robot

Complete locomotion of robot consists of two modes of motions: one is straight line motion and the other is sagging line motion. The complete working of the robot is as shown in Figure 4(a–f). Poses of robot P_1, P_2 and P_6 represent straight line motion configuration. During this motion, the swing unit is aligned in the vertical position and all wheels are lying on the same plane to give smooth forward or backward motion. The motion of the robot along a curved path refers to the sagging line motion, robot pose from P_2 to P_3 represent the crossing of the robot and poses from P_4 to P_5 represents the jumper cable motion. Transfer of the robot from the straight transmission line to the jumper cable is done with the aid of dual robotic arm and pulley mechanism. While crossing operation, one arm is held on the straight transmission line and other on jumper cable. Four nylon wires are fixed to each of the two arms. Four nylon wires are symmetrically fixed to the pulley mechanism system to balance the robot while crossing from straight from jumper cable or vice versa.

The robot is suspended from the straight transmission line and then lifted towards the jumper cable with the help of nylon-pulley mechanism. Detailed working of pulley mechanism is given in Section 2.3. Once the robot is lifted till the transmission line, the supporting wheel locks the robot on to the jumper cable. Then the driving and idle wheels get retracted and tighten to the jumper cable to traverse forward towards the dead-end of the jumper cable. And the same operation takes place when the robot is at the jumper cable to cross towards the straight transmission line.

2.2. Mobile robot base

The robotic base system provides support to the two swinging units. Each of the swinging units consists of a driving wheel, an idle wheel and a supporting wheel which act as a locking mechanism which prevents robot from falling. The supporting wheel helps in appropriate
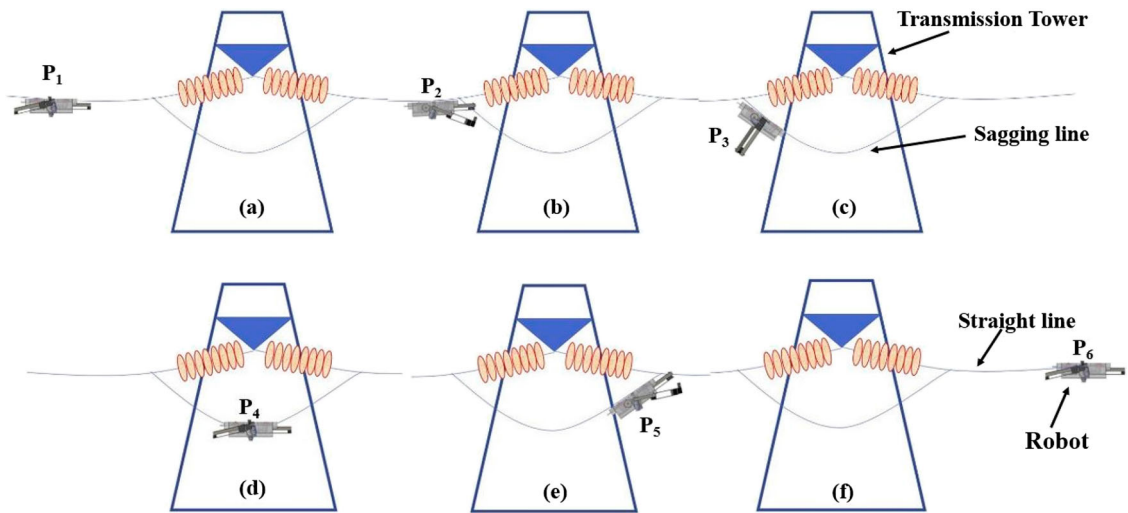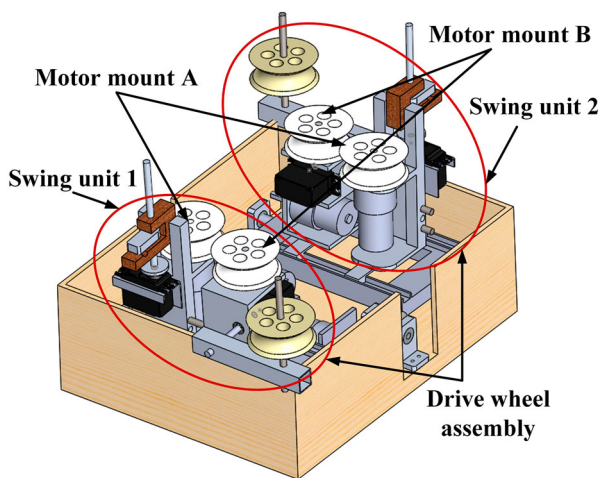
Figure 4. Working of the robot.

Figure 5. CAD model of mobile robot base system.

Figure 6. Front view and Side view of the swing unit.

locking and ensures safety measures. CAD Model of the mobile robot base system is shown in Figure 5.

2.2.1. Subsystems in robotic base system

Mobile robot base consists of two sets of swing units. The swinging mechanism is designed in such a way that the angular motion in a direction perpendicular to the transmission line for sagging line motion. This motion is made possible by coupling the swinging unit to the base via pillar coupling assembled with the radial ball bearing. Swinging unit is incorporated to provide inward and outward swing during the sagging line motion of the robot. The gripping on transmission line with the wheels is made possible by the use of engage–disengage mechanism. The retraction is controlled by using a timing belt pulley mechanism coupled to a threaded screw.

Drive wheel sub-assembly helps the robot to traverse on the transmission line. It comprises of 4 vertical axis wheels mounted on motor mounts A & B as shown in Figure 5. Mount A consist of driving wheel with driving motor assembly and mount B house idle wheel and
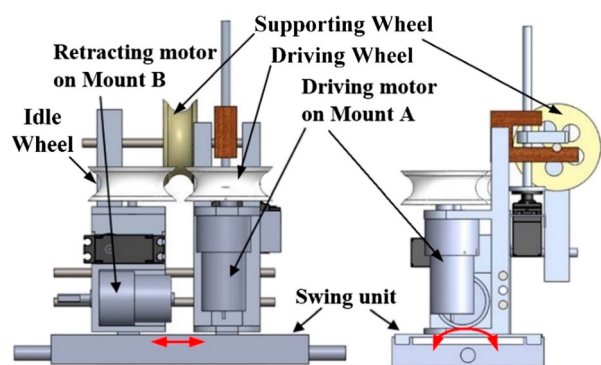
motors of engage-disengage mechanism. These mounts are placed on the slider plates which is on the swing unit as shown in Figures 6 and 7, giving pitching motion to bend inward and outward and sliding motion for engage–disengage mechanism of the motor mount. Set of two idle and driving wheels grip the transmission wire with the help of engage-disengage wheel mechanism and move forward with the help of a DC motor. The subassembly is designed symmetrical for perfect balancing. All the motors and wheels are placed crossed symmetrically to avoid unbalanced moment.

The engage-disengage mechanism is used to move the wheels away from each other. The motor driving the wheels is placed diagonally opposite side and sliding channel is provided on the base plate. Swing unit and engage-disengage mechanism are shown in Figure 7. Swing unit is made of base and sliding channel attached onto base via swing shaft. Control of flexibility is essential to provide proper traction over curved jumper wire. The swing unit will swing inwards during the sagging line motion of the robot.

Locking tab servo as shown in Figure 7, locks the end of supporting wheel shaft and minimizes instability of the robot once locked. It also bears shear load due to supporting wheel and the weight of entire
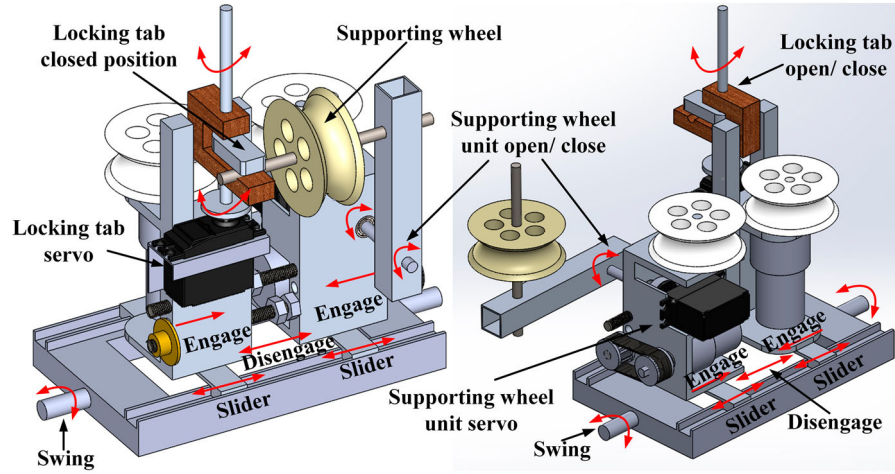
Figure 7. Supporting wheel closed and open position.
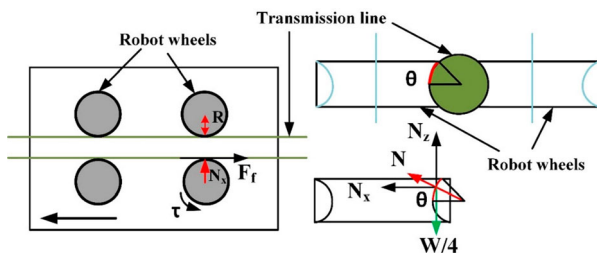

Figure 8. Top-view of the robot wheels and forces acting on the wheels.

robot which can hang on the supporting wheels without failure. Supporting wheel also ensures alignment of drive wheels parallel to the transmission line.

2.2.2. Design calculation of driving wheel motor torque

Gripping action of wheels on transmission line is achieved through the gripping force developed during the engaging of wheels by the motors and robot motion forward or backward is achieved through the driving wheel motor torque. It is assumed that robot is moving slowly. The driving wheel static torque is determined for the selection of actuators. Free body diagram of the wheel line assembly are shown in top and side views respectively in Figure 8 [45].

From the figure, at static equilibrium condition, $k N_z = mg$, where, k, m, g and N_z are the number of wheels $= 4$, mass of the robot, acceleration due to gravity and vertical force, respectively.

$$N = \frac{mg}{k \sin \frac{\theta}{2}} \tag{1}$$

$$N_x = N \cos \frac{\theta}{2} \tag{2}$$

where, N and N_x are the normal force and holding force, respectively.

Static torque of the motor, $\tau = F_f R = \mu N_x R$. Where, F_f is the frictional force for uniform velocity, μ is the co-efficient of friction, R is the radius of the wheel. Torque

calculation is carried out for diagonally opposite 2 driving wheels sets with $m = 15$ kg, $\theta = 50°$, Coefficient of friction for the rubber coating is taken as $\mu = 0.5$ and $R = 0.03$ m.

$N_{\text{final}} = nN$, $N_{x-\text{final}} = nN_x$ and $N_{z-\text{final}} = nN_z$. where, $n = 2$ wheels in one set.

N_{final}, $N_{x-\text{final}}$ and $N_{z-\text{final}}$ are calculated as 174 N, 158 N and 73.575 N respectively and Torque of the motor, τ is 2.375 Nm and by taking 1.5 factor of safety, the motor torque is 3.56 Nm. Motor is selected from the DC motor data sheet based on the actual torque of 4.58 Nm with 5 V, 7.5 A and 25 RPM. Only Static torque is considered for the selection of motors because the robot is moving at very low speeds.

2.2.3. Selection of wheel radius

The wheel profile is designed by considering many factors including the transmission line dimension as shown in Figure 9(a,b). These wheels are capable to hold the wires of different dimensions such as diameter, shape, single and multi-strand, and hence the holding radius varies from 0.00875 m to 0.0015 m. All wheels are nylon wheels because of the light weight and non-conducting electrical properties of nylon. The wheels are rubber coated to achieve better traction. Primary design consideration for wheels are that alignment of the wire should always be parallel to wheel profile, high torque transmission, high traction contact surface, need to apply and withstand high radial force.

2.2.4. Robot base chassis

Robot base chassis supports the swinging units, dual arm and the pulley system. This chassis consists of bottom plate and four vertical walls for covering the swinging units. The main consideration in robot base chassis design is the minimization of the weight for safe motion. The chassis is made up of Bakelite sheet in which bottom plate thickness is 0.008 m and vertical wall thickness is 0.004 m. Chassis base plate dimension is 0.42 × 0.22 m and vertical wall height of 0.05 m. The
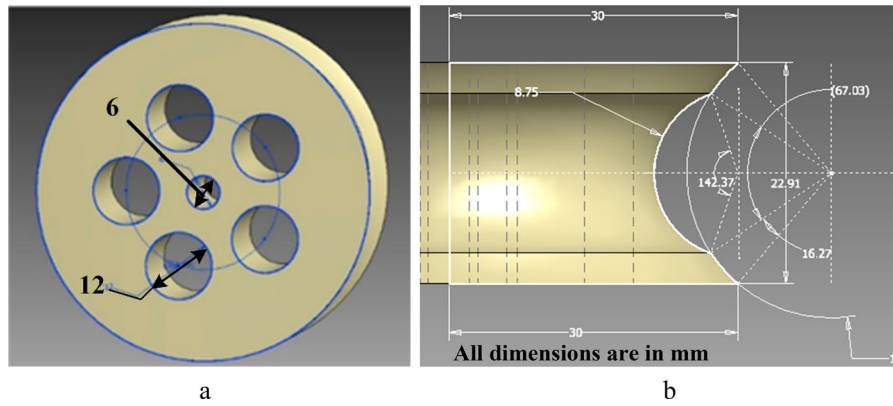
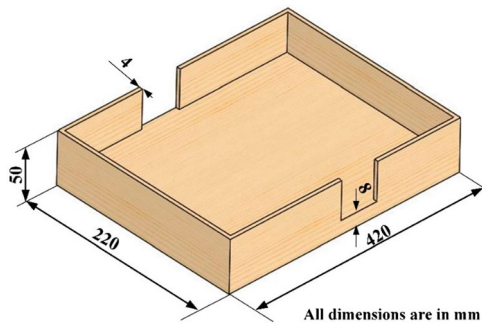**Figure 9.** (a) CAD models of the wheel. (b) Design specification wheels.

Figure 10. CAD model of the robot base chassis.

CAD model of robot base chassis after the optimized design is given in Figure 10.

Bakelite is rigid thermosetting plastic which is highly heat resistant insulator, light in weight, having higher strength and machinability. The robot has to manoeuvre through wires and cables without creating much sag. The complete static structural analysis for the determination of chassis dimensions is given in detail in Section 2.2.5.

2.2.5. Static structural analysis of robot chassis

The static structural analysis of the line inspection robot chassis mechanism is carried out using ANSYS. The maximum possible total load exerted by other subsystems on the robot base chassis is 15 kg. Hence the design load considered in this analysis is 150 N. The mechanical properties of the materials used for robot chassis, pulley system and dual arm are listed in detail in Table 1.

Static structural analysis of the robot chassis is carried out for the design load of 150 N in which the total load of 120 N is applied at the locations of swing units and pulley system. And the total load of 30 N is applied at the locations of arms in the chassis. Initially the model is made up of bakelite with base plate thickness of 0.008 m and wall thickness of 0.002 m. Then the structural analysis is carried out as per the above-mentioned loading conditions.

The deformation and the equivalent stress diagrams are given in Figure 11(a,b) respectively after the analysis. The simulation results show that the induced maximum deformation and stress are 0.000123 m and 23.548 MPa respectively.

Yield tensile strength of bakelite is 50 MPa. It is assumed that the safety factor is 2.5 for this chassis analysis. As per the safety factor, induced stress is higher than the yield strength of the bakelite and also the deformation is not safe. Hence, dimensions are changed and same modes of analysis are carried out for 16 sets of combinations for bakelite chassis using ANSYS Optimization tool for obtaining the final dimensions. Acceptable induced deformation of 0.078×10^{-3} m and stress values of 13.22 MPa are obtained. The deformation and stress analysis results are given in Figure 12(a,b) respectively. Hence, the thickness of the chassis base plate and vertical wall are selected as 0.008 and 0.004 m respectively with the safety factor of 2.5. The final base plate chassis and vertical plate dimensions are $0.42 \times 0.22 \times 0.008$ m and 0.05×0.004 m respectively.

2.3. Pulley mechanism

Pulley mechanism is designed for the robot to cross obstacles such as insulators, clamps, signalling spheres, vibration dampers, spacers, spiral bird diverters and tower junctions. The CAD model is as shown in Figure 13. The pulley mechanism is made up of four layers of single mechanism. The whole mechanism is supported at C clamp which is attached to the base system. The robot is made to move down using pulley mechanism and then by the aid of robotic arm the robot moves through jumper cable as explained in Section 2.1. Pulley mechanism is designed to facilitate vertical motion of the robot. This implies that the pulley should withstand the complete load of the robot. Four layered pulley mechanism is used to lift and suspend the robot during crossing operation and each layer consists of a spool timing belt pulley and motors.

Table 1. Mechanical Properties of material used [46].

Properties	Bakelite (Robot base chassis)	Aluminium (Pulley system & Arms)	Stainless Steel (All shafts in Pulley system & Arms)	Nylon (Wheels & Arm's nylon rod)	Mahogany Wood (Gripper hook)
Density (kg/m^3)	1360	2770	7750	1700	510
Yield Tensile Strength (MPa)	50	276	270	35	38
Young's Modulus (GPa)	17.2	71	193	3.5	9.6
Poisson's Ratio	0.32	0.33	0.31	0.39	0.35
Bulk Modulus (MPa)	–	69,608	169,300	–	420
Shear Modulus (MPa)	6520	26,692	73,664	1070	710
Ultimate tensile strength (MPa)	90	310	465	80	61

a
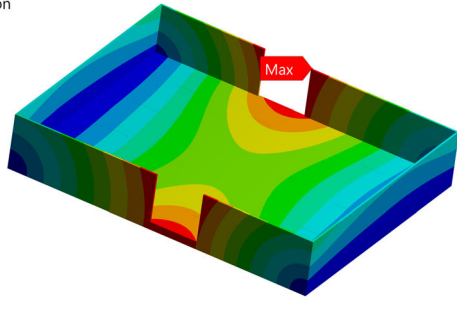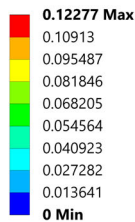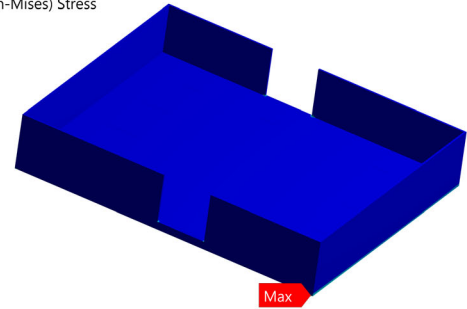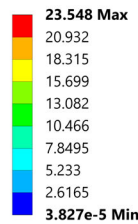
b

Figure 11. (a) ANSYS deformation (b). ANSYS Stress analysis.

a
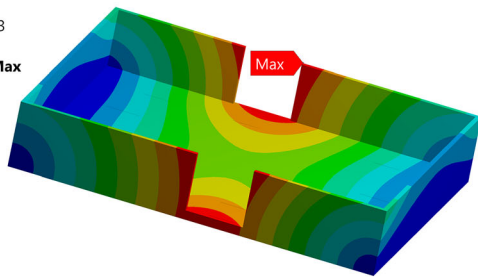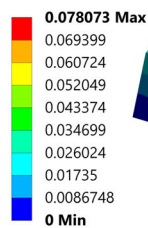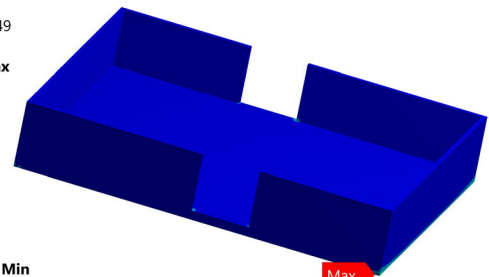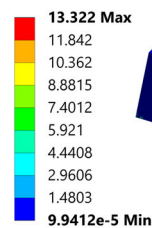
b

Figure 12. (a) ANSYS deformation (b). ANSYS Stress analysis.

2.3.1. Calculation of motor torque, diameter of spool-pulley and linear shaft based on static analysis

Static analysis is carried out for the determination of static torque required to lift the whole robot with the help of the pulley mechanism. Pulley mechanism is designed to carry a load of 150 N and the motors are chosen such that it can lift the robot. Schematic diagram of the pulley layer is as shown in Figure 14(a). It is understood that a torsional load is acting across the shaft of pulley mechanism. Considering factor of safety as 1.5, required torque of the motor is 2.59 Nm and based on availability in the market, the motor chosen is DC 4.58 Nm with peak current of 7.5 A and 25 RPM.

As mentioned in the previous section, pulley mechanism consists of four layers and each layer consists of two spool-pulleys which is mounted on the linear shaft. The diameter of spool-pulley is calculated and is designed with a consideration that the complete load acts on it, spool-pulley is as shown in Figure 14(b). However, the load is distributed among the eight spool pulleys. By comparing the volume of nylon wire to the volume of the spool slot where the nylon wire diameter is 0.001 m and slot width, t is 0.002 m and the outer radius, r_2 is 0.0175 m and the obtained inner radius, r_1 is 0.005 m.

Minimum diameter of the shaft is calculated using the von-mises (distortion energy) theories of failure.
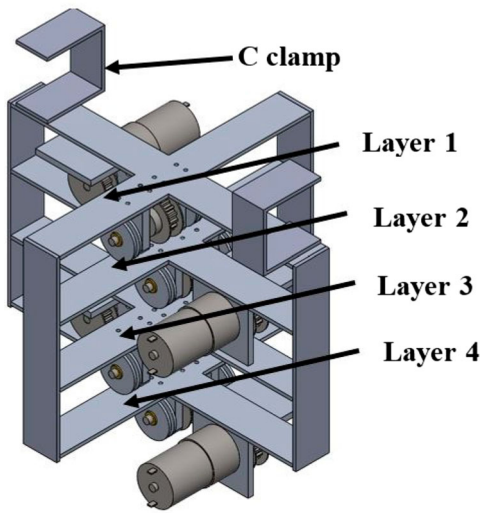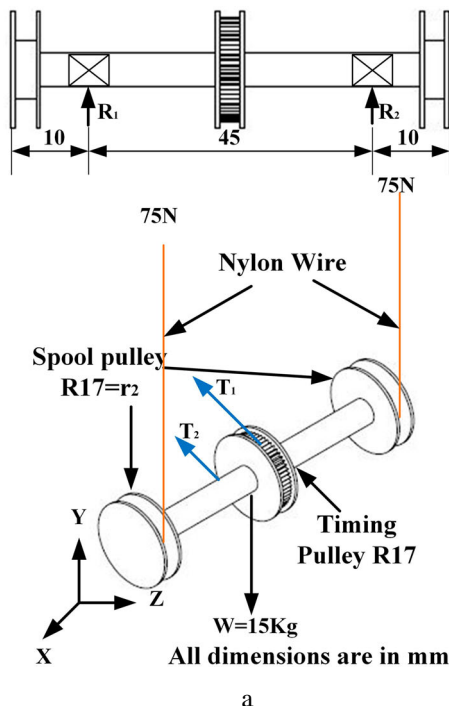
Figure 13. CAD model of 4-layer pulley system.

According to Max Shear Stress Theory,

$$\tau_{\max} = \sqrt{\left(\frac{\frac{32M_z}{\pi d^3}}{2}\right)^2 + \left(\frac{16T}{\pi d^3}\right)^2} \qquad (3)$$

For stainless steel material, Shear yielding stress, $\tau = \tau_{\max} = 125$ MPa, torque of the motor, $T = 4.077$ Nm, diameter of the shaft $= d$ and moment about Z axis, $M_Z = 2.5$ Nm. Taking factor of safety as 1.5 and substituting all the values in max shear stress theory, the designed diameter is 0.0091 m.

According to Distortion Energy Theory (Von-Mises and Henky theory),

$$\frac{S_{yt}}{FS} = \sqrt{\sigma_1^2 + \sigma_2^2 - \sigma_1\sigma_2} \text{ where}$$

$$\sigma_{1,2} = \frac{\sigma_x + \sigma_y}{2} \pm \sqrt{\left(\frac{\sigma_x + \sigma_y}{2}\right)^2 + \tau_{xy}^2} \qquad (4)$$

$$\sigma_x = \sigma_b = \frac{32M_z}{\pi d^3}, \tau_{xy} = \frac{16T}{\pi d^3} + \frac{W}{A} \qquad (5)$$

The yield strength of stainless steel $S_{yt} = 250$ MPa and factor of safety taken is 1.5. By substituting the values in the equations, the designed diameter is 0.00865 m. Considering the both theories the minimum diameter selected should be more than 0.0091 m so the next available diameter 0.01 m is selected.

2.3.2. Selection of timing belt pulley

Equipped with High torque DC geared motors (4 No's) and spools (8 No's) are provided on either side with slot in centre of mass. Robot mechanism is made symmetrical to avoid tilting of the robot to either side. There are two types of tension exerted such as:

Static Tension: By applying load, on the belt one can note down the deflection (ρ) and find θ.

Dynamic Tension: It is the tension which is created due to the torque applied on the pulley,

$$\frac{\tau}{r} + T = \frac{(\text{Ultimate strength of the belt})}{\text{Factor of Safety}} \qquad (6)$$

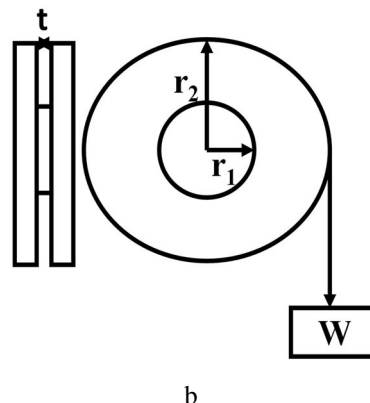Timing belt pulley dimensions are chosen by considering the constraints on the single layer of pulley system

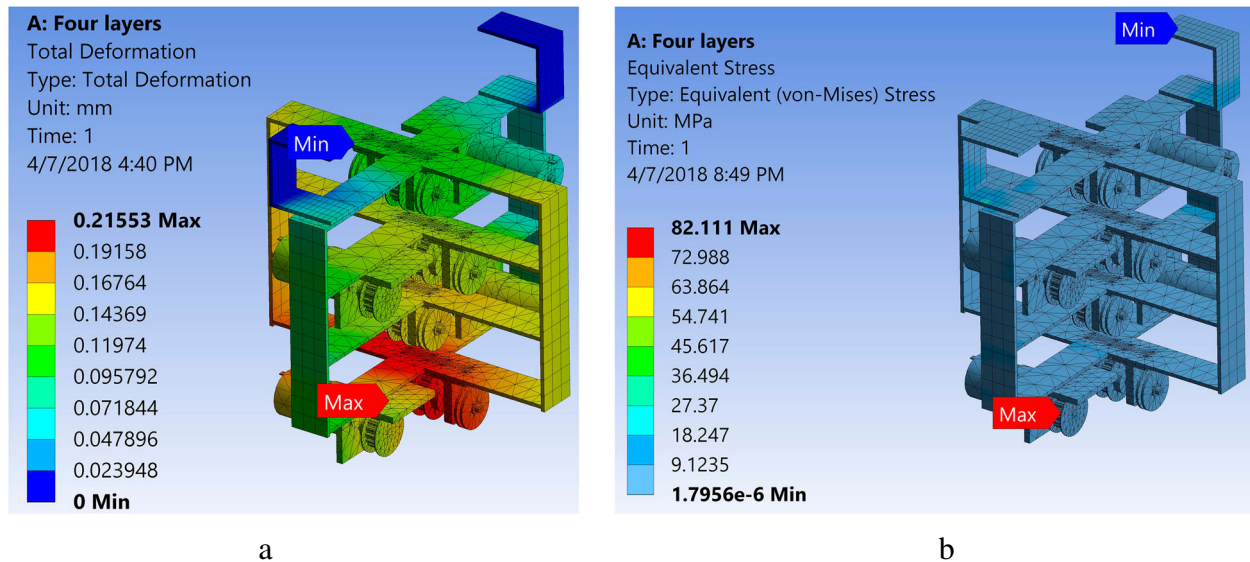**Figure 14.** (a) Pulley and spool pulley. (b) Spool pulley.

Figure 15. (a) Pulley mechanism deformation. (b). Pulley mechanism stress.

such as the radius of the pulley (r) is taken as 0.0015 m and the centre to centre distance (L) is 0.0056 m, the designed torque, τ is 3.5 Nm and taking factor of safety of the belt as 15. Specifications of aluminium timing pulley and metal reinforced rubber timing belt are P18XL037-6F and 80XL 09 mm with centre to centre distance of 55.9 mm respectively.

2.3.3. Static structural analysis of pulley mechanism

The pulley mechanism is fabricated using flat aluminium strips and is attached to the base by aluminium C-clamps. The maximum load acting on the pulley mechanism is due to the weight of the robot. Hence, the applied load is 150N. It is observed that the maximum deformation of 0.215×10^{-3}m is found at the spool as shown in Figure 15(a) and maximum stress induced is 82.11 MPa as shown in Figure 15(b). The yield strength of aluminium is 276 MPa which is higher than the maximum stress induced with safety factor 2.5. The deformation and stress induced are safe for this safety factor. Hence, the proposed design is safe.

2.4. Ten DoF dual arm

Crossing towers and other obstacles are the challenging tasks of the line inspection robot mechanism. Robot arm helps to transfer the gripper hook along with the nylon wires during crossing operation to the required goal position. Dual arm is a combination of two 5 DoF arms each on either side of the robot. CAD model of the dual arm robot with the base is shown in Figure 16.

2.4.1. Kinematic modelling of 10 DoF dual robot arm

Kinematic modelling helps in the synthesis of dual arm and also it gives the complete idea of motion behaviour of the mechanism. Crossing towers and other obstacles are the challenging tasks of the line inspection robot.
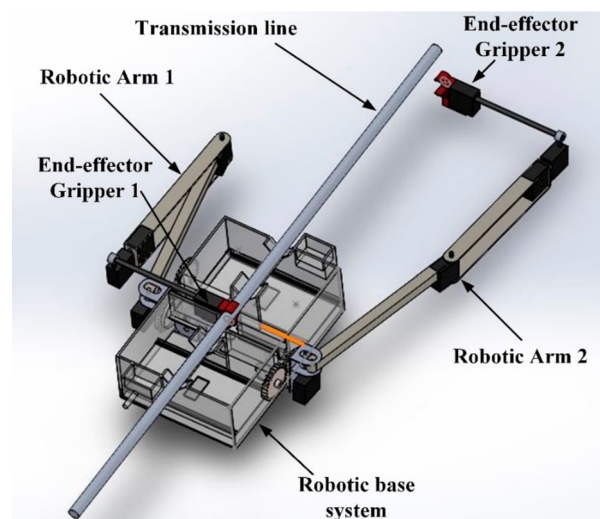
Figure 16. Conceptual CAD model of 10 DoF dual arm with robot base.

Dual arm and pulley systems are combined to perform this crossing task in the proposed work. It serves the robot to cross from a straight line to the jumper cable thus helping it in crossing a tower. There are two 5 DOF arm on either side of the robot, one to hold the straight transmission line and other on the jumper cable while crossing operation.

Modelling and analysis helps in designing a robot. Kinematic analysis can be carried out by considering following assumptions: (a) Mobile robot subsystems are rigid (b) Slipping between the wheel and the wire is neglected. (c) There exists enough friction between the wheels and the wire hence the wheels should be able to hold and move without disturbance. The robot consists of main body and dual arm for crossing the obstacles or junction wires/ropes.

The position and orientation of the end effector are obtained with respect to the known reference

Table 2. Joint link parameters of 5 DOF arm.

Link	a_i (m)	α_i	d_i (m)	θ_i
1	0	$-90°$	0	θ_1
2	L_1	0	0	θ_2
3	L_2	0	0	θ_3
4	0	$-90°$	d_1	$\theta_4 - 90°$
5	L_3	0	d_2	θ_5

frame from given joint link parameters. The standard Denavit-Hartenberg (DH) convention methodology is used for obtaining the joint link parameters. The DH parameters corresponding to each joint/link is given in Table 2. These DH parameters of dual 10 DOF arm are determined based on the frame assignment given in Figure 17.

Forward kinematic equations are derived using the DH parameters from the table. Final transformation matrix is determined and equated with the required pose for the determination of inverse kinematic equations. Closed form algebraic method is used for the determination of inverse kinematic analysis given in Equation (8).

$$\substack{B\\5}T = \substack{B\\0}T X \substack{0\\5}T = \substack{B\\0}T T_1^0 T_2^1 T_3^2 T_4^3 T_5^4$$

$$= \begin{bmatrix} n_x & o_x & a_x & p_x \\ n_y & o_y & a_y & p_y \\ n_z & o_z & a_z & p_z \\ 0 & 0 & 0 & 1 \end{bmatrix} \quad (7)$$

$\theta_1 = A \tan 2(r_{23}, r_{13}).$

$\theta_2 = A \tan 2(\tan \theta_5(C_1 n_x + S_1 n_y) + C_1 o_x + S_1 o_y),$
  $n_z \tan \theta_5 + o_z$

$\theta_3 = A \tan 2(L_1, L_2).$

$\theta_5 = A \tan 2(-S_1 n_x + C_1 n_y, -S_1 o_z + C_1 o_y)$

$\theta_1 = A \tan 2(r_{23}, r_{13}).$

$\theta_2 = A \tan 2(\tan \theta_5(C_1 n_x + S_1 n_y) + C_1 o_x + S_1 o_y),$
  $n_z \tan \theta_5 + o_z$

$\theta_3 = A \tan 2(L_1, L_2).$

$\theta_5 = A \tan 2(-S_1 n_x + C_1 n_y, -S_1 o_z + C_1 o_y).$

$\theta_{234} = A \tan 2(-a_3, C_1 a_x + S_1 a_y).$

where, $L_1 = -C_1 S_2 p_x - S_1 S_2 p_y - C_2 p_z$
  $+ 345 C_5(C_1 C_2 a_x + C_2 S_1 a_y - S_2 a_z)$
  $- 50(-S_2 C_1 a_x - S_2 S_1 a_y - C_2 a_z),$

$L_2 = C_1 C_2 p_x + S_1 C_2 p_y - S_2 p_z - 300$
  $- 345 C_5(-S_2 C_1 a_x - S_2 S_1 a_y - C_2 a_z)$
  $- 50 (C_1 C_2 a_x + C_2 S_1 a_y - S_2 a_z)$ and

$\theta_4 = \theta_{234} - \theta_2 - \theta_3$. Where, $L_1 = 0.3$ m, $L_2 = 0.21$ m, $L_3 = 0.345$ m, $d_0 = 0.01$ m, $d_1 = 0.085$ m,

$d_2 = 0.05$ m. $\quad (8)$

The dynamic analysis is carried out for the calculation of torques of various joints for the dual arm [47]. Motors are selected based on the joint torques, the motor with 1.5 Nm torque is feasible for the joint 1 which carries the load of the arm when it is in motion. Four servo motors (specification: High torque servo 1.67 Nm torque, 6 V) and 1 encoder motor (specification: 131:1 Metal Gear motor 37Dx57L mm with 64 CPR Encoder) are selected based on the torque calculated through dynamic analysis with safety factor of 1.5.

2.4.2. Static structural analysis of the robotic arm

The static structural analysis of the robotic arm is carried out at an instantaneous position at the sagging line when the robot is crossing from the transmission line to the jumper cable is as shown in Figure 18(a,b). The total weight of the robot is 15 kg including the battery and other electrical components. Hence, load of 150 N is applied on the robotic arm. It is observed that the maximum deformation of 0.00028 m is in the aluminium channel of second link and maximum stress induced is 156.79 MPa on the aluminium L-clamp. The yield tensile strength of the aluminium is 276 MPa which
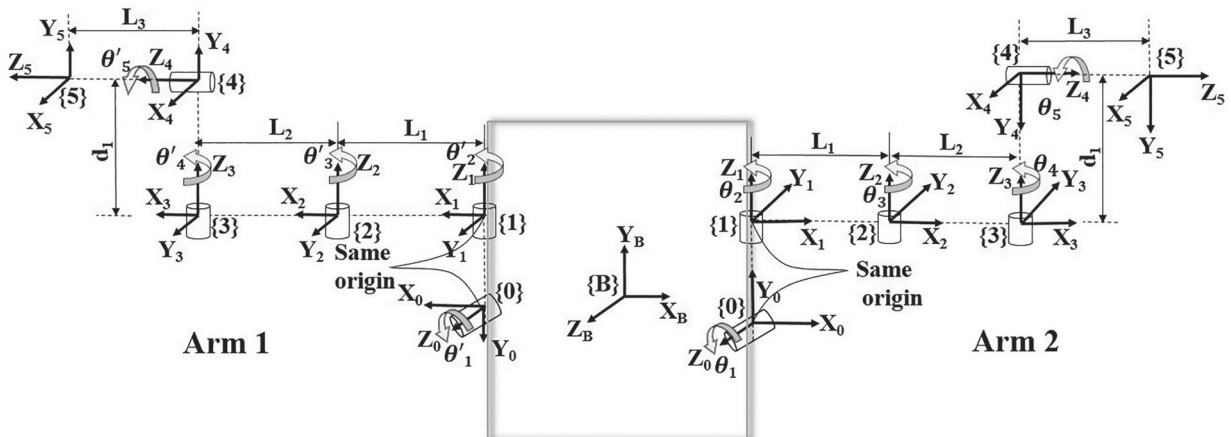
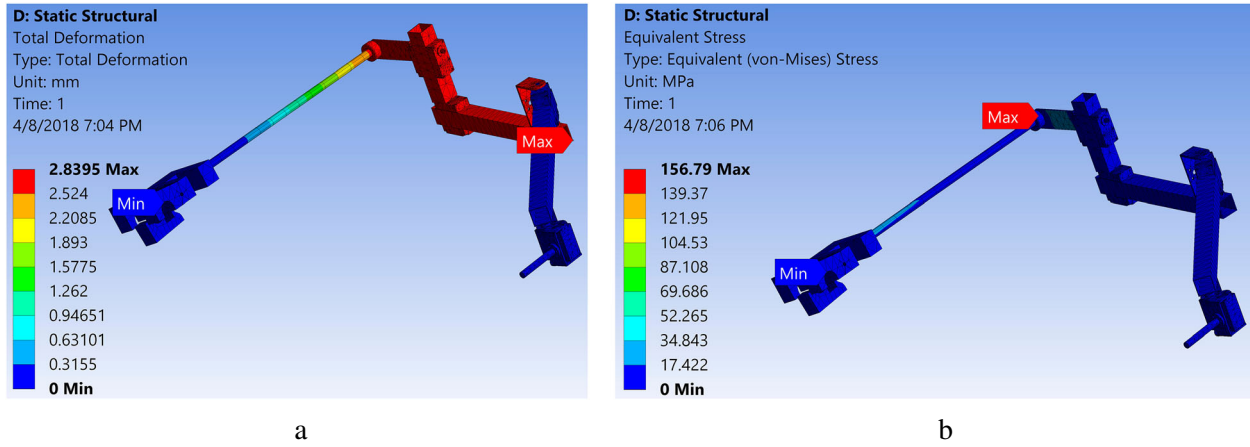**Figure 17.** Dual 10 DOF robotic arm frame assignment.

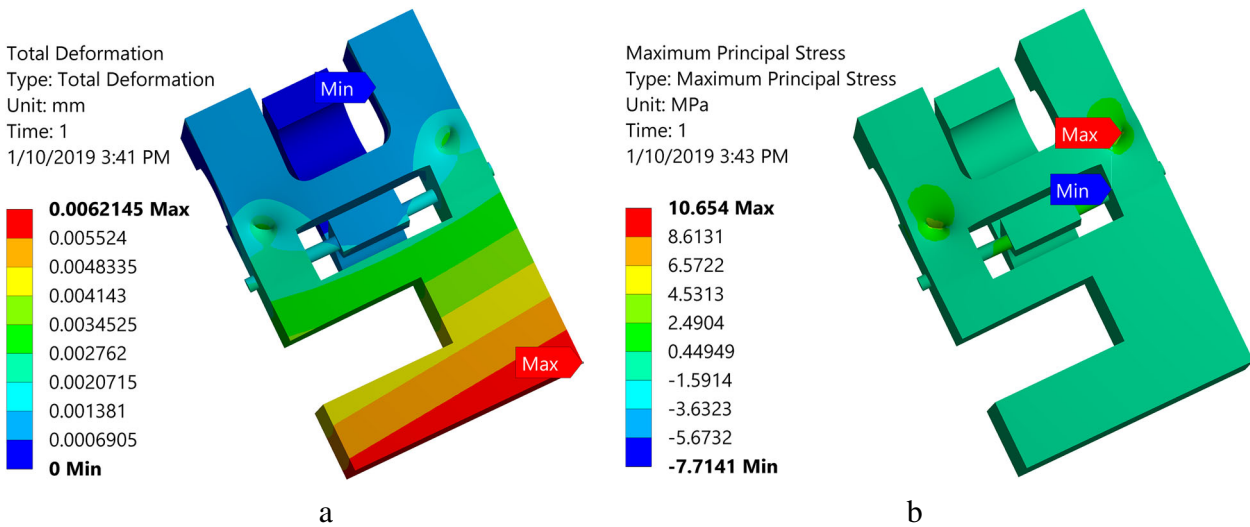**Figure 18.** (a) Arm deformation, (b) stress variation of arm.

Figure 19. (a) Deformation of the gripper. (b) Stress distribution of the gripper.

is higher than the maximum stress induced with the safety factor of 1.5. Cross-sectional dimension of the square channel is taken as 0.021 m based on the availability. The safety factor is assumed as 1.5 with internal wooden reinforcement. However, the analysis shown in the Figure 18(a,b) are without wooden reinforcement. Hence, deformation and stress induced are safe for this safety factor and the proposed design is safe with wooden reinforcement.

Static structural analysis of the gripper made up of Mahogany wood is analysed by applying a maximum load of 150 N for the determination of the final dimensions of the gripper. Number of iterations of structural analysis of the gripper with various dimensions are carried out for getting the safer deformation and stress for avoiding gripper failure during crossing. The maximum deformation and principle stress induced are 0.00621×10^{-3} m and 10.654 MPa respectively. The ultimate tensile strength of African Mahogany is 61 MPa which is higher than the induced stress after taking factor of safety of 2.5.

Gripper deformation and stress variations are shown in Figure 19(a,b) respectively. Since wood is a brittle
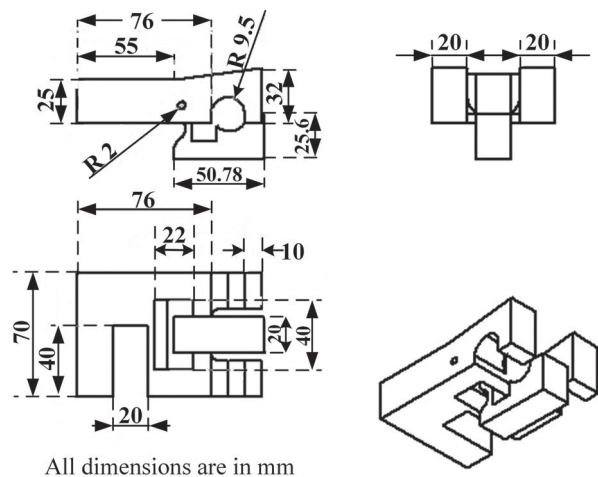

All dimensions are in mm

Figure 20. Dimensions of the gripper hook.

material, maximum principle stress is considered. The induced stress is less than the strength of Mahogany and hence the gripper design is safe. The final design of the gripper hook with all the dimensions is given in Figure 20.
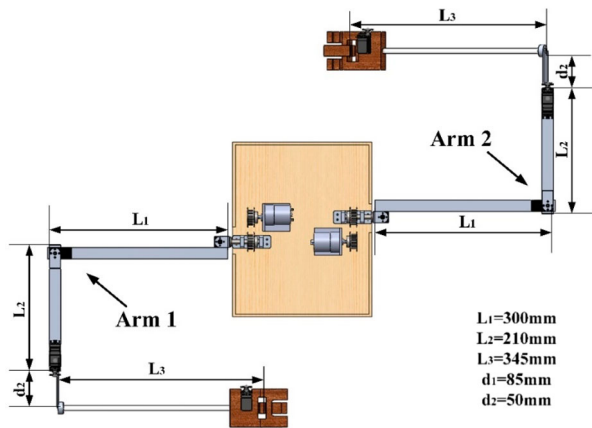
Figure 21. CAD model of 10 DoF dual arm after dimension selection.

Top view of the robot base with dual arm is shown in Figure 21 with all dimensions. All these dimensions are verified whether the arm length and degrees of freedom are sufficient to cross the obstacles and tower junctions with jumper cable by using V-rep (Virtual Robot Experimentation Platform). The arm motions from straight transmission line to the jumper cable are as shown in Figure 22 in V-rep.

3. Dynamic analysis of mobile base using ADAMS

Mobile base of the robot is equipped with dual arm when it traverses through straight line cable and jumper cable with or without obstacle during the inspection of transmission line. The proposed robot is moving in
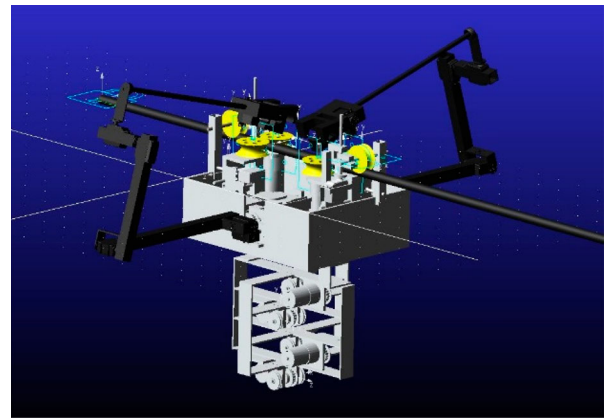

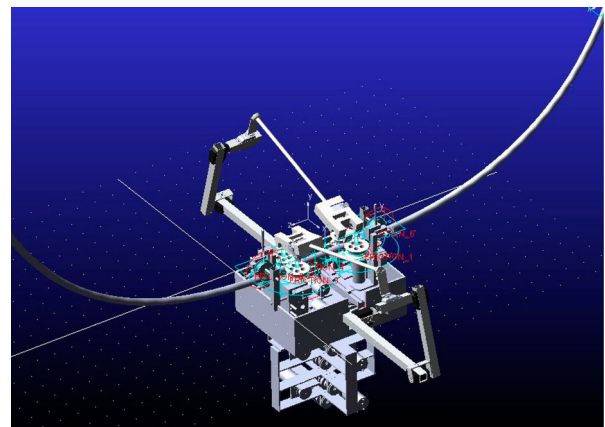**Figure 23.** Robot on straight transmission line in ADAMS platform.

Figure 24. Robot on jumper cable in ADAMS platform.

quasi static motion and hence static torque is determined in Section 2.2.2. The same robot can also be used for high-speed applications and hence dynamic analysis is also important to determine the dynamic torque.
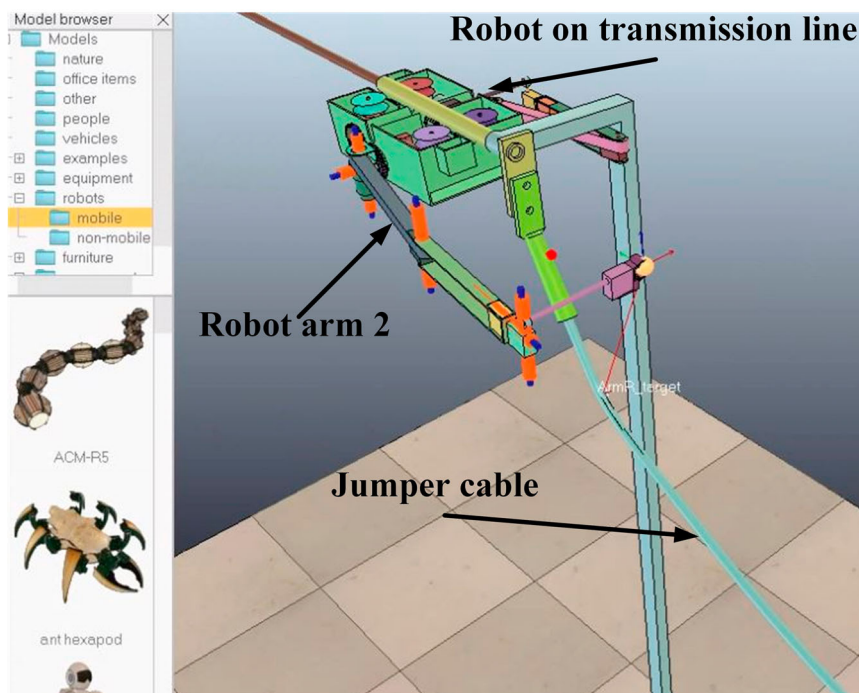

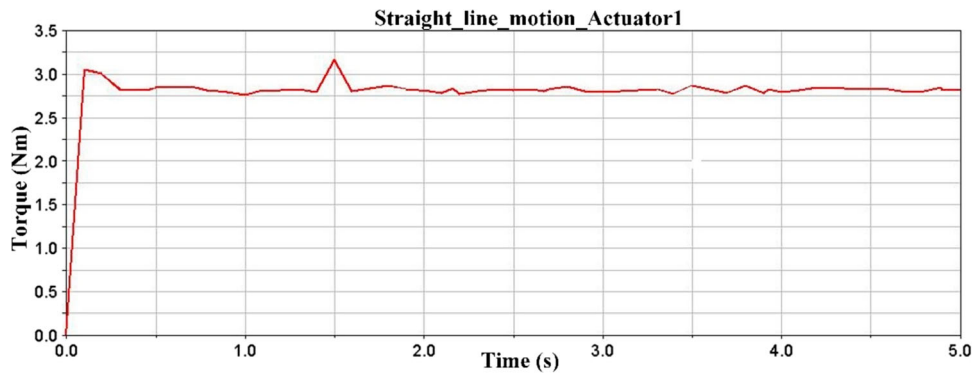**Figure 22.** Snapshot of V-rep validating.

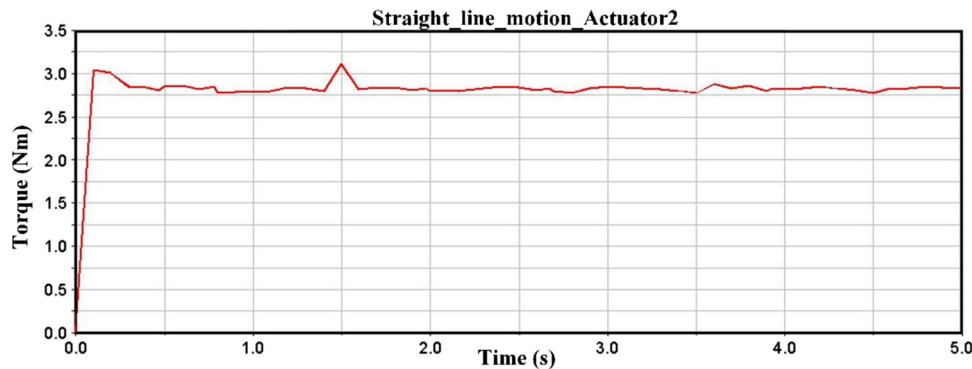**Figure 25.** Joint actuator torque at driving wheel of swing unit 1.

Figure 26. Joint actuator torque at driving wheel of swing unit 2.

ADAMS based dynamic analysis is carried out and torque variations are plotted during the straight-line motion for a speed of 0.05 m/s. The dynamic analysis of the robot while it is moving through straight transmission line and sagging jumper cable using ADAMS is shown in Figures 23 and 24 respectively.

Theoretical joint torques of the swing units 1 and 2 (Refer Figure 5) during the straight line motion are shown in Figures 25 and 26 respectively.

In Section 2.2.2, actual static torques of joints at swing unit 1 and swing unit 2 are same and is equal to 3.56 Nm. In dynamic analysis, the theoretical maximum joint torque at driving wheel of swing units 1 and 2 during straight-line motion are 3.15 and 3.1 Nm respectively. Actual dynamic maximum joint torque at swing units 1 and 2 are 4.095 and 4.03 Nm respectively with safety factor 1.3. This variation in the torque is due to the assumption that the centre of mass is assumed at the centre of the base platform and also it is assumed that swing units are symmetrical about the sagittal and frontal planes in statically stable condition. In actual dynamic case there will be shift of centre of mass from the centre of mobile base which is taken in account during the dynamic analysis. The variation in the torque values are acceptable because acceleration and friction effects are also considered in the dynamic analysis using ADAMS which are not considered in the case of static analysis.

Dynamic analysis is carried out and torque variations are also plotted during the sagging line motion for a speed of 0.01 m/s from bottom to the top most position of the sagging line. The dynamic torque at driving wheel of swing units 1 and 2 while moving through sagging line is shown in Figures 27 and 28 respectively.

The theoretical torque at the joint of driving wheel in swing unit 1 and 2 are 3.46 and 3.5 Nm respectively. Actual dynamic torque during the sagging line motion at the joints of swing units 1 and 2 are determined by taking a safety factor of 1.3. Hence, the actual torque at these joints at swing unit 1 and swing unit 2 are 4.49 and 4.55 Nm respectively. Actuators are already selected based on the actual static torque of 3.56 Nm. As per the data sheet, actuator with torque value of 3.56 Nm is not available in the market. Hence, actuator corresponds to the next higher torque value of 4.58 Nm is selected.

Specifications are given in Section 2.2.2. Data sheet torque is higher than the dynamic actual torque of 4.49 and 4.55 Nm at swing units 1 and 2 respectively during sagging line motion. Hence, the selected DC motors can also be used for operating the robot in dynamic conditions.

4. Assembled robot and control

All the sub-systems of the robot are fabricated as per the designed parameters and joint actuators are selected as per the static and dynamic analysis. Complete assembly of the robot is as shown in Figure 29. Fabricated robot base, dual arm, pulley system and other sub-systems are labelled in the figure. Robot base consists
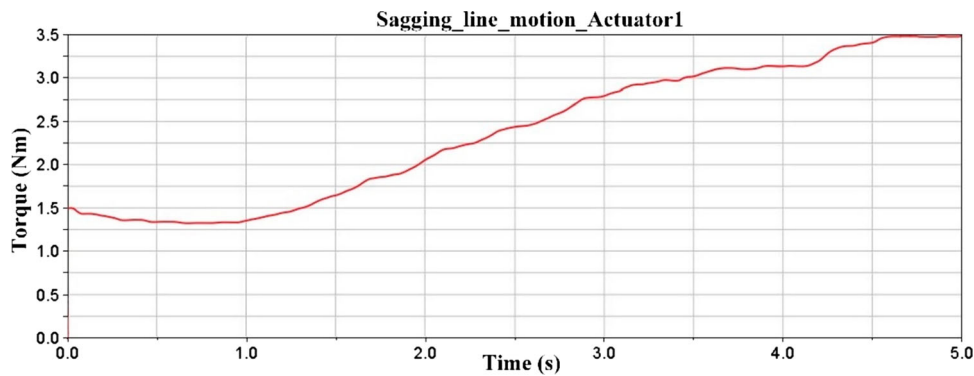
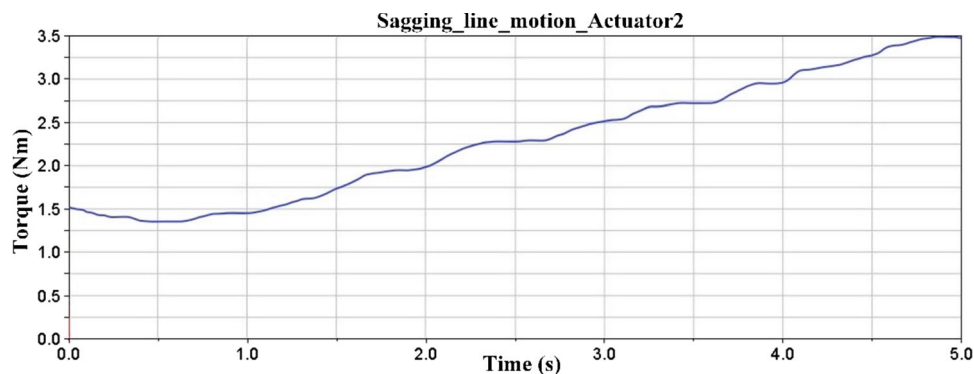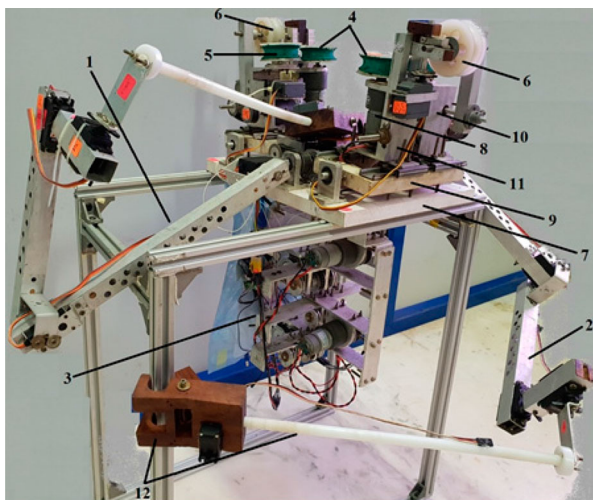**Figure 27.** Joint actuator torque at driving wheel of swing unit 1.

Figure 28. Joint actuator torque at driving wheel of swing unit 2.

1.Arm1, 2.Arm2, 3.Pulley system, 4.Driving wheels, 5.Idle wheels, 6.Supporting wheels, 7.Robot base chassis, 8. Driving motor, 9.Pitch plate/swing unit, 10.Motor mount A (Retracting part A), 11.Motor mount B (Retracting part B), 12.Nylon rod and gripper hook.

Figure 29. Complete assembly of the robot.

of two swinging units and each of them has a driving wheel, an idle wheel and a supporting wheel which helps to lock the robot appropriately and locking system avoids falling of robot from the transmission line. Driving and idle wheels helps in robot motion through straight transmission line and sagging jumper cable.

Ten DoF dual arm is fabricated as per the model given in Figure 3. It consists of two sets of five rotary joints and is made of square aluminium channel to make the arm lightweight. End-effector gripper is mounted on the nylon rod and is made up of Mahogany wood to grip the transmission wire.

Individual pulley system layer is made up of flat aluminium strips on which timing pulley, spools and DC motors are mounted and all these four layers are assembled on the vertical plate which is fixed to bottom of the robot base. Four layered pulley system is used to lift or suspend the robot with the help of nylon wire.

4.1. Smart phone based control of the robot

Arduino based controller is developed and implemented through smart phone-robot user interface which is shown in Figure 30. Robot controller is used for controlling the robot on an experimental tower setup with straight transmission line and jumper cable. In Figure 30, Screen 1 shows various keys for forward and backward motion through straight and sagging line. From the screen 1, "Arm 1" and "Arm 2" keys directs to screen 2 and "Pulleys" key directs to screen 3 for controlling four layers of pulley system.

The control architecture of the robot includes one Arduino Mega 2560 Microcontroller and two Arduino UNOs. Arduino Mega serves as the master controller of Arduino UNOs and each UNO aids the control of individual arms. The control architecture is depicted in detail in Figure 31.

Control of the main subsystems such as mobile robot base, pulley system and dual arm is established using the smart phone application named
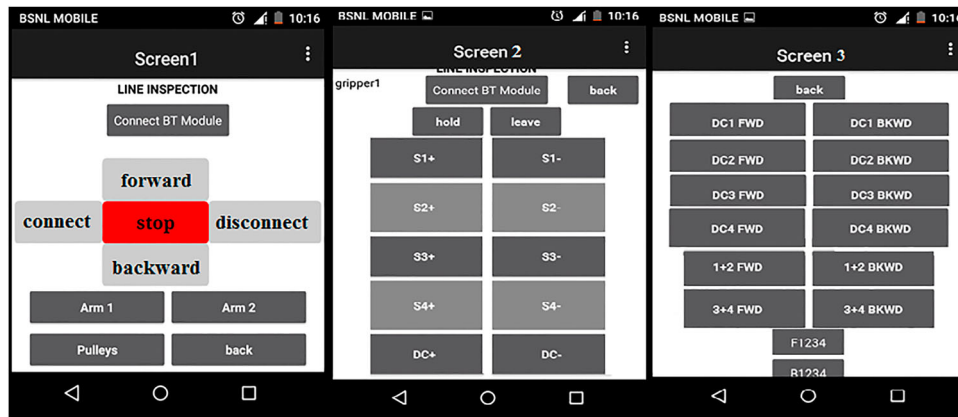
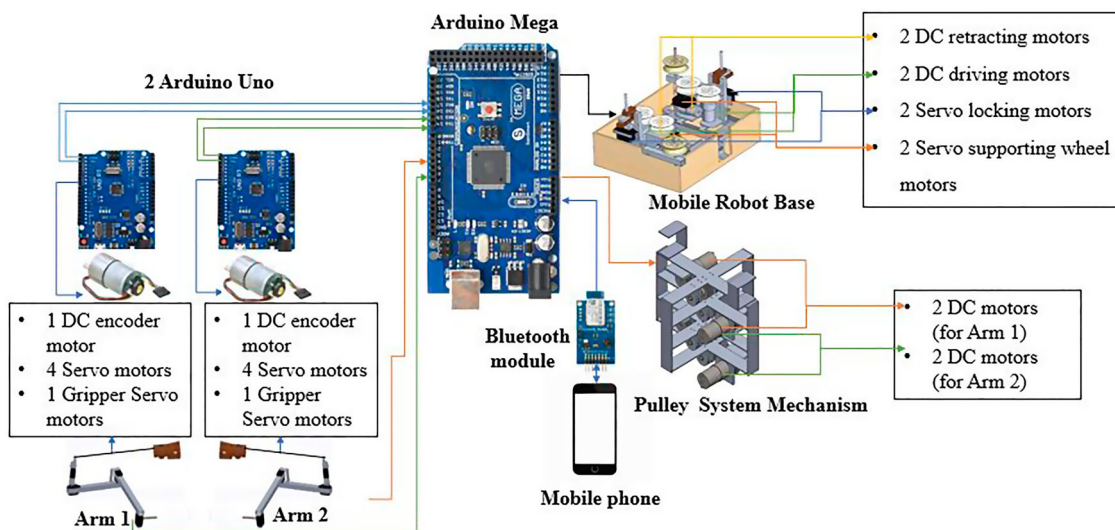**Figure 30.** Smart Phone-robot interface application.

Figure 31. Control architecture.

"Bot Controller" developed using MIT App Inventor which communicates with the Arduino Mega using Bluetooth module. All the tasks are controlled using corresponding buttons in the application interface.

The robot base consists of four DC motors, out of which two are used for engaging and disengaging the mounts A & B (Refer part 10 and part 11 in Figure 29), while the other two are used for driving the robot forward and backward. Also, the base consists of four servo motors which help the supporting wheel to lock and hang itself on to the transmission line. The robot holds the transmission line by engaging the mounts A & B after locking the supporting wheel and locking tab. Supporting wheel and locking tab are actuated with the help of supporting wheel motor and locking servos respectively. The two driving motors are placed on diagonally opposite mounts which adjusts themselves with the aid of the engage–disengage unit motors to hold on to the electric line. Both the driving wheels rotate in the same direction enabling it to move forward or backward as per the instructions given. The robot has also a swing mechanism where the platforms with mounts A & B adjust themselves to adapt to sagging electric lines.

The pulley system is used for lifting and lowering of the robot while crossing an obstacle or a tower junction. It comprises of four layers; each consists of one DC motor to which two nylon wires attached to the gripper. The first two layers are attached to Arm1 gripper while the other two to Arm 2 gripper. The dual arm is controlled by two Arduino UNOs which communicates with the master Arduino Mega serially. Each arm has five rotary joints which are driven by one DC encoder motor and four Servo motors. These motors rotate the joint to a specific angle to achieve the required pose to grab the transmission line.

The combined effort of the pulley and dual arm helps the robot to cross the tower junction or obstacles as explained in Section 2.1. All modes of motions including obstacle avoidance navigation and crossing tower junction are performed through the Smartphone application instructions given by the user.

5. Results and discussions

Design of the complete robot system is carried out based on the kinematic, static and dynamic analysis
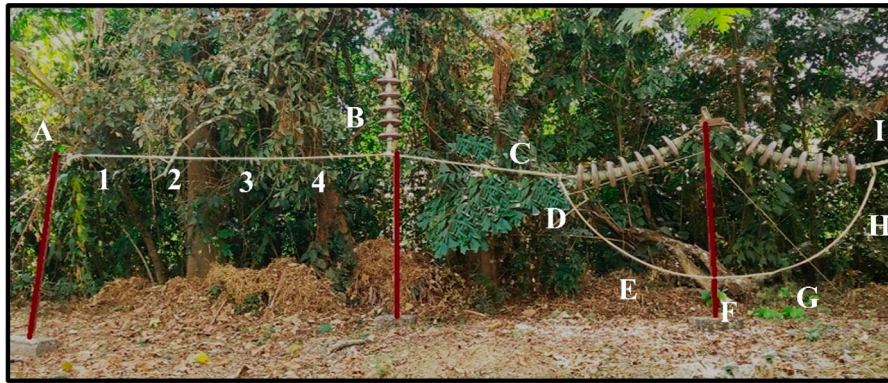
Figure 32. Experimental tower setup.

Figure 33. Testing of robot traversing on the straight transmission line: Snapshots.

Figure 34. Robot crossing the tower junction: Snapshots.

which are given in detail in the preceding sections. All subsystems of the robot mechanism are fabricated, assembled and integrated with the control system. Android-based control system is explained in Section 4.1. Robot-based experiments are conducted through straight line and jumper cable of a transmission line setup. These results are given in detail in this section.

5.1. Experimentation: motion of robot on straight transmission line, sagging jumper cable and crossing the tower junction

A suspension and tension tower setup is constructed for performing outdoor experiments. The experimental tower setup is given in Figure 32. A1234BC represents

Figure 35. Testing of robot motion on the sagging line: Snapshots.

Table 3. Time taken for various modes of motion by the robot.

| Sl. No | Time taken (s) | | | |
	Straight transmission line (A1234BC) with velocity 0.5 m/s	Crossing tower junction (CD)	Jumper cable (DEFGH)	Total time
1	20.40	42.02	6.42	68.84
2	20.32	42.12	10 (S) NC	72.44 (NA)
3	20.34	42.51	6.80	69.85
4	21.21	42.83	6.35	70.39
5	21.09	42.15	10 (S) NC	74.22 (NA)
6	20.90	42.73	6.71	70.34
7	21.20	42.24	9 (S) NC	72.44 (NA)
8	20.61	43.10	6.45	70.16
9	20.90	42.80	6.32	70.02
10	21.03	42.52	12 (S) NC	75.55 (NA)
Average	20.8	42.6	6.5	69.9
Where, S = Slipping, NC = Not Considered and NA = Not Applicable				

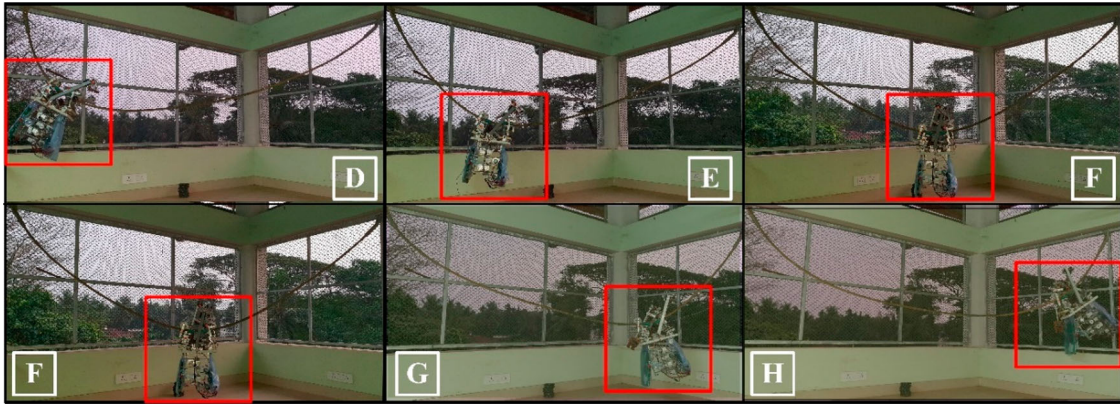the straight transmission line cable, CD and HI indicates the crossing of tower junction between straight line and jumper cable and DEFGH represents jumper cable in the figure. Robot motion through straight line, tower junction crossing and motion through jumper cable are shown in Figures 33–35 respectively.

Ten trial experiments are conducted. The average time taken for ten experiments is determined. Distance from point A to point B is 10 m and B to C is 2 m which are set for the robot to traverse through straight transmission line. Average time taken by the robot is 20.8s for straight line motion A to C. Crossing operation of tower junction from C to D takes an average time of 42.6 s.

Crossing is performed slowly compared to the straight line motion because the sagging jumper cable is just 1 m above the ground level and due to the issue of slipping. Also, robot is touching the ground during the crossing operation. Hence, experimentation of jumper cable motion is conducted in the indoor laboratory set up as shown in Figure 35. The sagging line slope and span in indoor setup is same as the outdoor standard tower setup. Friction pad on the driving wheel is slipped slightly four times out of 10 experiments at the top most position of the jumper cable during the sagging line motion. This is mainly due to the looseness of friction pad at the gripper. Average time taken for the motion DEFGH is 6.5 s for an approximate span of 3 m in 6 non-slipping indoor experiments. Experimental

snapshots are given in Figure 35. The total average time taken for the straight line motion, crossing operation and jumper cable motion is 69.9 s for all the non-slipping 6 experiments. The time taken for motion through jumper cable is not varying as expected due to looseness of friction pad.

The time taken for straight line motion, tower crossing and jumper cable motion are given in detail in Table 3.

Time taken during the experimentation from the point A to H is 69.9 s which is deviated from the desired average time of 30 s. This variation is mainly due to the slight misalignments of subsystems in the robot during the fabrication. Also, there are some problems in the fabricated tower setup. These issues can be reduced through precised fabrication of the complete robot and the tower setup.

The sole problem faced during the testing is slipping of the wheel friction pads from the sagging line, which will be rectified in the succeeding phase of the work. Initial phase of the robot development has been completed and various stages of the experimentations are depicted in this paper. Integration of sensors and other subsystems for online inspection will be carried out in the next phase of the work. A comparison of important robot mechanisms with their weight, dimensions and major remarks are listed in Table 4.

Proposed mobile dual arm robot mechanism is light in weight, compact and low cost which is capable

Table 4. Line inspection robot: A comparison.

Sl. No	Name of the Robot and Country	Weight (kg)		Dimension (m³) Length × Width × Height (L × W × H)	Remarks
1	Mobile dual arm robot (Proposed robot in this paper)		12	0.42 × 0.22 × 0.5	• Suitable for both tension and suspension towers. • Compact and light in weight. • Low cost.
2	Line Scout [10–12], Canada		112	1.37 × 0.85 (L × H)	• Not suitable for tension tower crossing. • Robot is heavy.
3	Expliner [13], Japan		90	1.5 × 1.3 × 1.5	• Not Suitable for single power lines and tension towers. • Difficult to travel on steep cables. • Complex design with counterweights and heavy.
4	Cable crawler [14], Zurich		58	1.2 × 1.2 × 1.2	• Traverses only on single guided wires, Hence, no obstacle is crossed. • Robot is heavy.
5	Biped line walking robot [15], Hamburg		30 kg (Approx.)	0.8 × 0.1 (H × W)	• Unable to cross bigger obstacles and steep tension tower junctions.
6	Hybrid robot [16], China		8	0.65 × 0.065	• Lesser flight-time. • Difficult to take-off and to land while crossing the towers and obstacles. • Difficult to operate in bad weather conditions.
7	An inspection robot [17], Georgia, USA		13.7	0.43 × 0.24 × 0.33	• Crosses only smaller obstacles however tested only on straight and sagging transmission line. • Not tested for tower junction crossing.
8	Three mobile robots [18], China	PIR	15.2	0.51 × 0.27 × 0.156	• Traverses through straight line with obstacles however cannot cross tower junctions.
		TIR	44.8	0.91 × 0.42 × 0.816	• Can cross both obstacles and tower junctions with separate attachment in the tower setup. • Robot is heavy.
		CIR	56.6	0.95 × 0.42 × 1.1	• Traverses on the transmission line with tower junctions and can cross all types of obstacles by mimicking the behaviour of animals. • Robot is heavy.
9	An inspection robot [19], Mongolia		NA	Not Available (NA)	• Robot prototype is not tested and implemented in the real time.
10	A mobile robot [20–36], China		30	0.76 × 0.3 × 0.67	• Robot is heavy.
11	An autonomous inspection robot [37–41], China		30	1.2 × 0.8 (L × H)	• Robot is focused on supporting navigation along an inclined line with unstable counterbalancing. • 13 Degrees of freedom to imitate monkeys motion and to avoid obstacles. • Robot is heavy.
12	A mobile robot [42], Brazil		NA	Not Available (NA)	• The robot cannot cross the obstacles.
13	An inspection robot [43,44], South Africa		10 +payload 10	0.64 × 0.45 × 0.2	• Tested only in indoor environment. • 20 kg is the overall weight of the robot including the payload of 10 kg.

of traversing through suspension and tension towers with obstacle crossing capability. The features of this robot mechanism are clear from the comparative table given above. The weight of the robot is approximately 12 kg with all accessories and within the volume of $0.42 \times 0.22 \times 0.05 \text{m}^3$.

6. Conclusions and outlook

Robot mechanism is developed and tested in a combined mode of tension and suspension towers. All the subsystems of the robot are designed and actuators are selected as per the detailed design procedure based on kinematic, static and dynamic analysis of the robot. Each subsystem of the robot is fabricated and tested individually. Then integration of all subsystems of the robot is carried out to achieve a compact robot mechanism. Android-based arduino controller is used for the indoor and outdoor experimentations. Proposed robot mechanism is a simple, novel, low cost and small in size design for traversing through both straight transmission line and jumper cable with the ability of crossing obstacles and tower junctions. This robot overcomes several limitations of other available inspection robots

as depicted in Table 4. A methodology of crossing obstacles and tower junctions is proposed in this paper. Robot performance is also analysed experimentally both in indoor and outdoor setup. The time taken for the robot motion is more than the expected duration due to the lack of precision in the fabricated robot and experimental tower setup. This work can be extended in following ways such as complete automation of the robot, real-time inspection through sensor integration, performance analysis of robot on real-time inspection, ground control of robot through trans-receiver module through various controllers, IOT-based inspection and identification of power theft through appropriate sensor integration. Proposed robot mechanism shall be an appropriate solution for the inspection and maintenance of widespread transmission lines, wire traversing robot based inspection of suspension, mine inspection and material transport to inaccessible locations for automated construction.

Disclosure statement

No potential conflict of interest was reported by the authors.

Funding

ORCID

C. M. Shruthi http://orcid.org/0000-0001-5041-0495
A. P. Sudheer http://orcid.org/0000-0003-0644-3702
M. L. Joy http://orcid.org/0000-0002-0282-5028

References

[1] Alexander LM, Mangum OK. Maintenance of transmission lines by helicopter. Electr Eng. 1953;72(12):1094.

[2] Wilton GS, Ormiston TS, Allan RA. Modern transmission-line maintenance. Proc Inst Electr Eng. 1967; 114(7):925–932.

[3] Dunlap JH, Van Name JM, Henkener JA. Robotic maintenance of overhead transmission lines. IEEE Trans Power Delivery. 1986;1(3):280–284.

[4] Sawada J, Kusumoto K, Maikawa Y, et al. A mobile robot for inspection of power transmission lines. IEEE Trans Power Delivery. 1991;6(1):309–315.

[5] Transmission & Distribution World. [Internet]. Powered by Informa USA, Inc. [2018 Jun 21]. Available from: http://www.tdworld.com/transmission/iran-utility-addresses-insulator-contamination/.

[6] Xu FY, Wang XS, Cao PP. Design and application of a new wheel-based cable inspection robot. In IEEE International Conference on Robotics and Automation (ICRA; 2011 May 9. p.4909–4914.

[7] Seok KH, Kim YS. A State of the art of power transmission line maintenance robots. J Electr Eng Technol. 2016;11(5):1412–1422.

[8] Gonçalves RS, Carvalho JC. Review and latest trends in mobile robots used on power transmission lines. Int J Adv Rob Syst. 2013;10(12):1–14.

[9] Toussaint K, Pouliot N, Montambault S. Transmission line maintenance robots capable of crossing obstacles: State-of-the-art review and challenges ahead. J Field Robot. 2009;26(5):477–499.

[10] Pouliot N, Montambault S. Geometric design of the linescout, a teleoperated robot for power line inspection and maintenance. IEEE International Conference on Robotics and Automation; 2008 May 19; Pasadena, California, USA. p. 3970–3977.

[11] Pouliot N, Montambault S. Field-oriented developments for linescout technology and its deployment on large water crossing transmission lines. J Field Robot. 2012 Jan;29(1):25–46.

[12] Pouliot N, Richard PL, Montambault S. Linescout technology opens the way to robotic inspection and maintenance of high-voltage power lines. IEEE Power Energy Technol Syst J. 2015;2(1):1–11.

[13] Debenest P, Guarmieri M. Expliner – from prototype towards a practical robot for inspection of high - voltage lines. 1st IEEE International Conference on Applied Robotics for the Power Industry (CARPI 2010), Montreal, QC, Canada; 2010 Oct 05–07. p. 1–6.

[14] Buringer M, Berchtold J, Buchel M, et al. Cable-crawler-robot for the inspection of high-voltage power lines that can passively roll over mast tops. Indust Robot Int J. 2010;37(3):256–262.

[15] Wang L, Liu F, Xu S, et al. Design, modelling and control of a bipedal line-walking robot. Int J Adv Rob Syst. 2010;7(4):33.

[16] Chang W, Yang G, Yu J, et al. Development of a power line inspection robot with hybrid operation modes. IEEE/RSJ International Conference on Intelligent robots and systems (IROS); 2017 Sep 24–28; Vancouver, BC, Canada. p. 973–978.

[17] Miller R, Abbasi F, Mohammadpour J. Power line robotic device for overhead line inspection and maintenance. Indust Robot Int J. 2017;44(1):75–84.

[18] Fan F, Wu G, Wang M, et al. Multi-robot cyber physical system for sensing environmental variables of transmission line. Sensors. 2018;18(3146):1–29.

[19] Byambasuren BE, Kim D, Oyun-Erdene M, et al. Inspection robot based mobile sensing and power line tracking for smart grid. Sensors. 2016;16(250):1–14.

[20] Li T, Lijin F, Hongguang W. Development of an inspection robot control system for 500KV extra-high voltage power transmission lines. Proceedings of the IEEE SICE 2004 Annual Conference; 2004 Aug 4; (2). p.1819–1824.

[21] Wang L, Fang L, Wang H, et al. Development and control of an autonomously obstacle-navigation inspection robot for extra-high voltage power transmission lines. Proceedings of the IEEE SICE-ICASE International joint Conference; 2006 Oct 18. p. 5400–5405.

[22] Wang L, Wang H, Fang L. Obstacle-navigation control of power transmission lines inspection robot. Proceedings of the IEEE International Conference on Robotics and Biomimetics, ROBIO; 2007 Dec 15. p. 706–711.

[23] Hongguang W, Yong J, Aihua L, et al. Research of power transmission line maintenance robots in SIACAS. Proceedings of the 1st IEEE International Conference on Applied Robotics for the Power Industry (CARPI); 2010 Oct 5. p. 1–7.

[24] Yifeng S, Hongguang W, Lie L. Research on the influence of the driving wheel and robot posture on climbing capability of a transmission line inspection robot. Proceedings of the 6th IEEE Conference on Industrial Electronics and Applications (ICIEA); 2011 Jun 21. p. 1632–1639.

[25] Song Y, Wang H, Jiang Y, et al. AApe-D: A novel power transmission line maintenance robot for broken strand repair. IEEE Proceedings of the 2nd International Conference on applied Robotics for the power Industry (CARPI); 2012 Sep 11. p.108–113.

[26] Fu SY, Zhang YC, Cheng L, et al. Motion based image deblur using recurrent neural network for power transmission line inspection robot. Proceedings of the International joint Conference on Neural Network; 2006 Jul 16. p. 3854–3859.

[27] Siyao F, ZiZe L, Zengguang H, et al. Vision based navigation for power transmission line inspection robot. Proceedings of the IEEE 7th International Conference on Cognitive Informatics; 2008. p. 411–417.

[28] Yang G, Li E, Fan C, et al. Modeling and control of a bibrachiate inspection robot for power transmission lines. IEEE International Conference on Mechatronics and Automation (ICMA); 2010 Aug 4. p. 1036–1041.

[29] Song Y, Wang L, Jiang Y, et al. A vision-based method for the broken spacer detection. IEEE International Conference on Cyber Technology in Automation, Control, and Intelligent Systems (CYBER); 2015 Jun 8. p. 715–719

[30] Gongping W, Xiaohui X, Du E, et al. Kinematics and dynamics simulation of inspection robot for power transmission line. Proceedings of the 5th WSEAS International Conference on Signal Processing, Robotics and automation; 2006 Feb 15. p. 70–76.

[31] Wu G, Xiao X, Lai Y. A wheel-claw hybrid manipulator and its grasping stability for the mobile robot rolling/crawling along flexible cable. IEEE International Workshop on Robotic and Sensors Environments. ROSE; 2007 Oct 12. p. 1–6.

[32] Wu G, Zheng T, Xiao H, et al. Navigation, location and non-collision obstacles overcoming for high-voltage power transmission-line inspection robot. IEEE International Conference on Mechatronics and Automation, ICMA; 2009 Aug 9: p. 2014–2020.

[33] Wu G, Cao H, Xu X, et al. Design and application of inspection system in a self-governing mobile robot system for high voltage transmission line inspection). IEEE power and Energy Engineering Conference. APPEEC Asia-Pacific; 2009 Mar 27. p. 1–4

[34] Wu G, Xiao H, Xiao X, et al. Transmission line inspection robot and deicing robot: Key technologies, prototypes and applications. IEEE 1st International Conference on Applied Robotics for the Power Industry (CARPI); 2010 Oct 5. p. 1–6.

[35] Wei W, Yucheng B, Gongping W, et al. The mechanism of a snake-like robot's clamping obstacle navigation on high voltage transmission lines. Int J Adv Rob Syst. 2013;10(9):1–14.

[36] Fu WX, Wu G, Zhou P, et al. Energy-consumption estimation of inspection robot based on Kalman filter. J Zhejiang Univ (Eng Sci). 2015;4:9.

[37] Ren Z, Ruan Y. Planning and control in inspection robot for power transmission lines. Industrial Technology. ICIT 2008. IEEE International Conference; 2008 Apr 21. p. 1–5.

[38] Li Z, Ruan Y, Zhang F. A new posture plan for the inspection robot capable of clearing obstacles in power transmission line maintenance. Power and Energy Engineering Conference. APPEEC 2009. Asia-Pacific; 2009 Mar 27. p. 1–4.

[39] Jian J, Guoxian Z, Tingyu Z. Design of a mobile robot for the innovation in power line inspection and maintenance. Reconfigurable Mechanisms and Robots, 2009. ReMAR 2009. ASME/IFToMM International Conference; 2009 Jun 22. p. 444–449.

[40] Jin J, Zhu H, Zhang G. Counterweight-navigation of a mobile inspection robot working on the ground wires. In Automation and Logistics, 2009. ICAL'09. IEEE International Conference; 2009 Aug 5. p. 278–282.

[41] Li Z, Ruan Y. Autonomous inspection robot for power transmission lines maintenance while operating on the overhead ground wires. Int J Adv Rob Syst. 2010;7(4):25.

[42] Pinto AV, Sebrao MZ, Lourenco CR, et al. Remote detection of internal corrosion in conductor cables of power transmission lines. Applied Robotics for the Power Industry (CARPI), 2010 1st International Conference; 2010 Oct 5. p. 1–6.

[43] Lorimer T, Boje E. A simple robot manipulator able to negotiate power line hardware. Applied Robotics for the Power Industry (CARPI), 2012 2nd International Conference; 2012 Sep 11. p. 120–125.

[44] Rowell T, Boje E. Obstacle avoidance for a power line inspection robot. Applied Robotics for the Power Industry (CARPI), 2012 2nd International Conference; 2012 Sep 11:p. 114–119.

[45] Shruthi CM, Sudheer AP, Joy ML. Kinematic and static analysis of mobile dual Arm robot traversing through A multi-Stranded wire. Proceedings of the 2017 The 5th International Conference on control, Mechatronics and Automation; ACM, 2017 Oct 11. p. 1–6.

[46] American Society for Testing and Materials. Annual Book of ASTM Standards: International [Internet]. [2018 Jun 1]. Available from: https://www.astm.org/Standards/category_index.html.

[47] Shruthi CM, Sudheer AP, Joy ML. Modeling, analysis and Trajectory planning of a 5 Degree of freedom robotic Arm for a transmission line crossing robot. CAD/CAM, Robotics and Factories of the Future; 2016; Springer, New Delhi. p. 509–522.